Institutional Repository - Research Portal
Dépôt Institutionnel - Portail de la Recherche
researchportal.unamur.be
University of Namur

RESEARCH OUTPUTS / RÉSULTATS DE RECHERCHE

Description of Non-Covalent Interactions in Benzyl Chalcocyanate Crystals from Smoothed Cromer-Mann Electron Density Distribution Functions

Leherte, Laurence; Bodart, Laurie; Wouters, Johan; Vercauteren, Daniel

Published in:
Journal of physics. Condensed matter

DOI:
10.1088/1361-648x/ac99c9

Publication date:
2022

Document Version
Peer reviewed version

Link to publication

Citation for pulished version (HARVARD):
Leherte, L, Bodart, L, Wouters, J & Vercauteren, D 2022, 'Description of Non-Covalent Interactions in Benzyl Chalcocyanate Crystals from Smoothed Cromer-Mann Electron Density Distribution Functions', *Journal of physics. Condensed matter*, vol. 34, no. 49, 494003. https://doi.org/10.1088/1361-648x/ac99c9

General rights
Copyright and moral rights for the publications made accessible in the public portal are retained by the authors and/or other copyright owners and it is a condition of accessing publications that users recognise and abide by the legal requirements associated with these rights.

- Users may download and print one copy of any publication from the public portal for the purpose of private study or research.
- You may not further distribute the material or use it for any profit-making activity or commercial gain
- You may freely distribute the URL identifying the publication in the public portal ?

Take down policy
If you believe that this document breaches copyright please contact us providing details, and we will remove access to the work immediately and investigate your claim.

Download date: 02. May. 2026

Submitted to Journal of Physics: Condensed Matter

Description of non-covalent interactions in benzyl chalcocyanate crystals from smoothed Cromer-Mann electron density distribution functions

Laurence Leherte, Laurie Bodart, Johan Wouters, Daniel P. Vercauteren

Laboratory of Structural Biological Chemistry, Unit of Theoretical and Structural Physical Chemistry, Department of Chemistry, NAmur Research Institute for LIfe Sciences (NARILIS), Namur Institute of Structured Matter (NISM), NAmur MEdicine & Drug Innovation Center (NAMEDIC), University of Namur, Rue de Bruxelles 61, B-5000 Namur (Belgium)

Email: laurence.leherte@unamur.be
ORCID: 0000-0001-8468-5462

The present research paper is our contribution in memory and honour of Enrico Clementi outstanding personality and prestigious career. LL and DPV have had the great chance to be invited by and collaborate with Enrico during numerous research stays particularly in Poughkeepsie, Kingston, Strasbourg, Cagliari, and Como. Among all our collaborations, one of his many ideas in his "Global simulation" scheme (cfr. notably in IJQC, 42, 547, 1992) concerned the importance of non-covalent interactions in solid state or life science systems, which we are tackling in the present work.

Abstract

A well-known method to characterize non-covalent interactions consists in the topological analysis of electron density distribution (EDD) functions, complemented by the search for minima in the reduced gradient density (RDG) distributions. Here, we characterize intermolecular interactions occurring in crystals of benzyl chalcocyanate compounds through bond critical points (BCP) of the promolecular electron density (ED) built from the crystallographic Cromer-Mann parameters, at several smoothing levels t. The trajectories formed by the t-dependent BCP locations are interpreted in terms of the intermolecular interactions occurring within the crystal arrangements. Chalcogen…nitro BCPs are clearly present in the unsmoothed EDDs but are annihilated as t increases, while chalcogen…chalcogen BCPs appear and are among the only BCPs left at the highest smoothing level. The chalcogen bonds are differentiated from the other chalcogen interactions through the linear chalcogen…BCP…nitro geometry at low smoothing level and their more negative Laplacian values. The annihilation of CPs can be followed by the apparition of a RDG minimum, associated with a very weak interaction. Along the BCP trajectories, the Laplacian shows a progressive concentration of the ED in the intermolecular space within the crystals and adopts the most negative values at the shortest atom…atom separations. At the termination point of a BCP trajectory, the drastic increase of the ellipticity value illustrates the flattening of the EDD.

Keywords

promolecular electron density, smoothing, reduced density gradient, critical points, non-covalent interactions, crystal benzyl chalcocyanates

Introduction

Since the fundamental and influential work of R. Bader about the topology of electron density distribution (EDD) functions [1], numerous developments have been brought to the analysis of non-covalent interactions (NCIs) such as hydrogen [2], halogen, chalcogen, and pnictogen bonds [3,4]. All are directional and may possibly be competitive interactions with comparable strength properties [5,6].

Promolecular EDDs have long been considered as good models in chemical bond analyses [7,8], molecular-similarity applications [9], crystal density analyses [10], and molecular surface calculations [11,12]. Such ED descriptions have also been considered as a way to correct atom-based electrostatic interaction energies [13].

Several papers report on the absence of a direct relation between the ED topology and chemical concepts such as the chemical bond [14-16]. It is likely due to the fact that promolecular EDDs, i.e., built from non-interacting atoms, present some common characteristics with quantum mechanics (QM) EDDs, at the level of the critical points (CPs) and bond paths [7,8,14,17]. In their recent comparative study, Keyvani et al. conclude that small deformations originating from the interactions between atoms can affect the topology of an EDD [14]. Taylor also reports that similarity between promolecular and *ab initio* QM EDDs is one of the multiple arguments against the idea that bond paths and their CPs depict bonding interactions [16]. Saleh et al. studied differences between low temperature experimental and promolecular EDDs [18]. They also concluded that despite the information decrease in the promolecular model, there is a one-to-one correspondence between the NCIs detected in an experimental and a promolecular EDD. Second, they observed that the intermolecular EDD is reasonably well approximated by a promolecular model, while strong interactions may lead to more significant ED topology changes [18]. Indeed, a promolecular ED representation based on spherical and independent atoms cannot depict effects of, e.g., asphericity and electron delocalization between atoms. It is not N-representative, i.e., it does not contain the information needed to derive a proper quantum mechanical wavefunction. It is a subject which is largely discussed within the field of quantum crystallography [19-21].

The Quantum Theory of Atoms in Molecules (QTAIM) developed by R. Bader allows to investigate peculiar non-bonding and bonding intramolecular situations. As examples, Bader and Matta showed the absence of bond paths at the level of short C-Ti distances [22]. Thus, close atoms do not necessarily lead to the presence of a bond path. It also allows to confirm the presence of

bond paths between distant atoms which are considered to be non-bonded, e.g., between hydrogen atoms bearing identical or similar charges [23].

In the present work, we limit our investigations to intermolecular regions of the EDDs. We use an already described approach suitable for the construction [24] and analysis of Gaussian type EDDs at various levels of smoothing [25,26]. Gaussian-based functions present the great advantage to allow fast and analytic ways to provide ED-derived properties such as similarity indices [24,27,28], convolution products [29,30], and topological quantities based on ED first and second derivatives. The method is applied here to crystal structures of small molecules interacting through chalcogen bonds [25,26]. Particularly, analytical promolecular EDD functions are built from the Cromer-Mann (CM) approximation of QM scattering factors. For each atom type, the scattering factors are easily computed from the tabulated coefficients that are commonly implemented in crystallography softwares. They present the advantage to be available for a large set of elements [31].

Four benzyl chalcocyanate structures were selected, i.e., *p*-nitrobenzyl thiocyanate (CSD code CIGGII), *p*-nitrobenzyl selenocyanate (CSD code CIGGEE), *p*-nitrobenzyl tellurocyanate (CSD code NOTECN), and benzyl selenocyanate (CSD code CIGGOO) [32,33]. With the aim to go beyond a single analysis of distance-based contacts, through an analytical and fast calculation method, the results are interpreted in terms of interaction types as they evolve with the smoothing degree of the EDD function. Chalcogen bonds were differentiated from other non-covalent interactions and specific descriptors have been suggested. In the next section, we first describe how the CPs in a progressively smoothed EDD are located. Then details regarding the implementation of the analytical expression for the CM-based EDD are given. In the Results section, the CP trajectories along the smoothing degree are described and assessed in terms of intermolecular interactions.

Methods

a. Critical points and reduced density gradient

CPs are points where the gradient of the EDD is zero. The so-called bond CPs (BCPs) are characterized by two negative ($\lambda 1$ and $\lambda 2$) and a positive ($\lambda 3$) eigenvalues of the local Hessian matrix $\boldsymbol{H}$ (a matrix built on the local second derivatives of the ED). They are located between two ED maxima. In an unsmoothed EDD, the BCPs are located between covalently bound atoms, but

can also be observed between non-covalently bound atoms such as at the level of intermolecular atom…atom interactions [34]. The ring CPs (RCPs) are characterized by one negative ($\lambda 1$) and two positive ($\lambda 2$ and $\lambda 3$) eigenvalues of $\boldsymbol{H}$. They generally corrrespond to ED minima within ring structures.

The sign of the Laplacian $L = \sum_{i=1}^{3} \lambda_i$ that is associated with a CP provides information on the local concentration ($L < 0$) or depletion ($L > 0$) in the ED. The sign of $\lambda 2$ is considered as an indicator of the bonding ($\lambda 2 < 0$) or non-bonding ($\lambda 2 > 0$) character of the CP [35]. Another property of interest is the ellipticity $\varepsilon = \frac{\lambda 1}{\lambda 2} - 1$ of the EDD at a BCP. It is usually related to the bond order at the BCP as it allows to evaluate the accumulation of the ED in a plane [36].

In a previous work [25,26], we used the iterative Newton-Raphson algorithm to locate the CPs in a molecular EDD function expressed as a summation over atomic Gaussian functions according to:

$$\boldsymbol{r}_{CP(\mathrm{n+1})} = \boldsymbol{r}_{CP(\mathrm{n})} - \delta\, \boldsymbol{H}_n^{-1}\, \nabla\rho(\boldsymbol{r}) \qquad (1)$$

where $\boldsymbol{r}$ is the position vector of the CP, n, the iteration step number, δ, the allowed displacement, $\boldsymbol{H}_n$, the Hessian matrix at step n, and $\nabla\rho(\boldsymbol{r})$, the gradient of the ED $\rho(\boldsymbol{r})$.

In a NCI approach, the EDD is analyzed so as to identify extended regions of space where the reduced density gradient (RDG) function $s(\boldsymbol{r})$ approaches zero [3,37,38]:

$$s(\boldsymbol{r}) = \frac{|\nabla\rho(\boldsymbol{r})|}{2(3\pi^2)^{1/3}\rho(\boldsymbol{r})^{4/3}} \qquad (2)$$

Thus, at the CP locations, the function $s(\boldsymbol{r})$ is zero. Particularly, the BCPs and RCPs, which are characterized by negative and positive $\lambda 2$ values, point to the so-called bonding and non-bonding sites, respectively. The regions surrounding BCPs and RCPs are characterized by low but non-zero values of $s(\boldsymbol{r})$ [18]. To search for the RDG-based NCIs, we adopted a flood-filling type algorithm that is described in a previous paper [25,26]. In the present work, RDG grids were built with a grid step of 0.1 Å and a spatial cutoff criteria chosen to select RDG holes located in the intermolecular interaction regions only, i.e., in a distance range of 0.8 to 3.5 Å from the selected molecular structure.

b. Smoothed Cromer-Mann electron density distributions functions

The CM coefficients, obtained by fitting versus QM X-ray scattering factors, allow to analytically evaluate such factors for free atoms and ions according to a nine-coefficient expression:

$$f\left(\frac{\sin\theta}{\lambda}\right) = c + \sum_{i=1}^{4} a_i \, e^{-b_i \left(\frac{\sin\theta}{\lambda}\right)^2} \quad (3)$$

where 2θ is the X-ray scattering angle and λ, the wavelength. The corresponding atomic EDD function is obtained as the Fourier transform (FT) of *f*. Particularly, the FT of the constant *c* is a delta function centered at the atom position, while the FT of the four Gaussian functions in Equation 3 are also Gaussian functions. In such a context, the parameters b_i in Equation 3 are inversely proportional to the width of their corresponding EDD Gaussian function, i.e., a narrow EDD contribution is associated with a low value of b_i. In the direction of the incident X-ray beam (θ = 0°), *f(0)* is equal to the number of electrons.

In a previous paper, Equation 3 was approximated by a combination of Gaussian functions only [39]:

$$f_{fit}\left(\frac{\sin\theta}{\lambda}\right) = \sum_{i=1}^{4} a'_i e^{-b'_i \left(\frac{\sin\theta}{\lambda}\right)^2} \quad (4)$$

where the coefficients *a'* and *b'* were obtained by fitting Equation 4 to the original Equation 3. In such a way, the EDD of an atom is also a combination of four Gaussian functions. The model is named *cm_fit* further in the text.

Equation 4 can be easily smoothed, at any smoothing degree *t*, through a convolution product with another Gaussian function [29]:

$$\rho(r) = \sum_{i=1}^{4} a'_i \left(\frac{4\pi}{b'_i}\right)^{3/2} \frac{1}{\left(1 + 8\frac{2\pi^2}{b'_i} t\right)} \, e^{\left(\frac{-4\pi^2 r^2}{b'_i \left(1 + 8\frac{2\pi^2}{b'_i} t\right)}\right)} \quad (5)$$

Such an expression can be seen as the solution to a diffusion equation, where the smoothing factor t is the product of a diffusion coefficient D multiplied by the time. It has also been shown that t is mathematically equivalent to the crystallographic concept of overall isotropic displacement parameter $<u^2>$ [39]. Both descriptions explain that t has area units. On the whole, smoothing corresponds to a spread of the EDD which preserves the total number of electrons. For large atoms such as Se and Te, the fit expressed by Equation 4 is not fully satisfying, i.e., the f values at small angles are not properly approximated (Figure SI1). As numerical illustrations, the residual standard deviation between Equations 3 and 4 for Te and Se is 0.6118 and 0.4170, respectively, while it is only 0.0410 and 0.0071 for lighter atoms such as S and O, respectively. Consequently, another approximation procedure for the atomic EDD function was followed.

First, at $t = 0$ bohr^2, removing the parameter c from Equation 3 affects the ED values only at the atom position since the EDD is a delta function. It is thus assumed that neglecting this term does not significantly affect the interatomic BCPs properties. Consequently, Equation 5 is then used to calculate ρ, a' and b' being replaced by a and b, respectively. The model is named *cm_trunc* further in the text. As example, a comparison of the unsmoothed EDD calculated for the atom pair O…N separated by a distance of 2.70 Å (as in a hydrogen bond), using the fitted parameters a' and b' (Equation 4) and considering the original CM parameters excluding c, is illustrated in Figure 1. At the O and N positions, the respective higher and lower peaks obtained with the *cm_trunc* model versus the *cm_fit* one are due to the neglect of the negative and positive values of c for N and O. Contrarily, at the BCP location, the differences in the position coordinate x, the ED ρ, the eigenvalue $\lambda 2$, the Laplacian L, and the ellipticity ε are less significant. Particularly, one obtains x = 1.328 and 1.330 Å, ρ = 0.01278 e/bohr^3 in both cases, $\lambda 2$ = -0.01181 and -0.01193 e/bohr^5, L = 0.05038 and 0.05110 e/bohr^5, and ε = 0 in both cases, for the *cm_fit* and *cm_trunc* cases, respectively.

Second, at $t > 0$, the parameter c can not be neglected since the peaks of the EDD are not located on the atoms any longer [25]. To overcome the problem, Equation 3 is considered to be a sum over five Gaussian terms, with $a_5 = c$ and $b_5 = 0$. However, Equation 5 is not strictly applicable when b_i' *(or* b_i*)* = 0. Nevertheless, at the limit $b_5 \rightarrow 0$, the corresponding EDD function term simplifies to:

$$\rho_5(r) = a_5 \left(\frac{1}{4\pi\, t}\right)^{3/2} e^{\left(\frac{-r^2}{4\pi\, t}\right)} \quad (6)$$

The resulting analytical expression of the EDD function based on the CM parameters is thus a combination of Equation 5, that is applied to the CM pairs (a_i, b_i) i = 1 to 4, and Equation 6 applied to the last pair (a_5, b_5). The model is named *cm_lim* further in the text and is relevant only at values $t > 0$ bohr^2. Figure 2 illustrates the evolution of the absolute differences $\Delta\rho$, $\Delta\lambda 2$, and ΔL for sulfur (an atom for which the *cm_fit* model is reliable) [39] with the smoothing degree t. The differences are all lower or equal to 10^{-3} starting at $t = 0.3$ bohr^2. Differences are small at even lower values of t in the case of an interatomic BCP. Indeed, differences observed at the BCP of the N…O atom pair are all lower than 10^{-4}, at $t = 0.1$ bohr^2 and beyond.

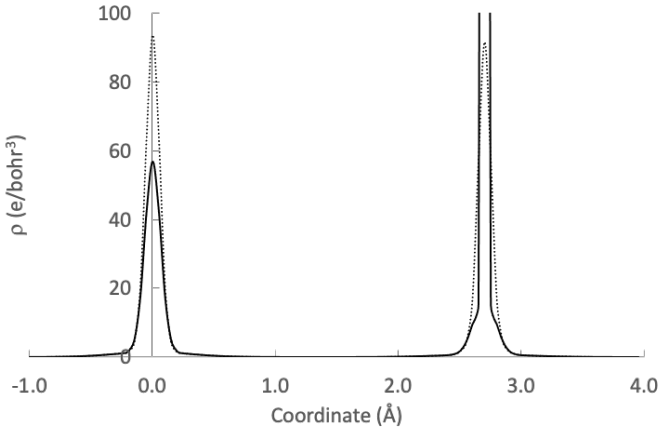

Figure 1. Superimposition of the unsmoothed EDD along the O…N axis as obtained using the *cm_fit* (plain line) and *cm_trunc* (dotted line) models.

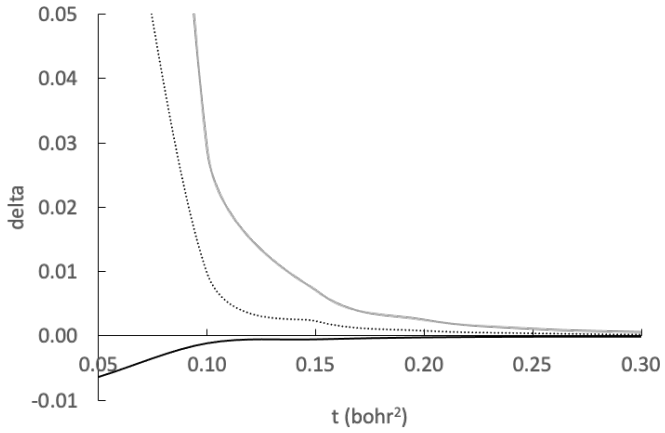

Figure 2. Difference (delta) between ρ (e/bohr^3; black plain line), $\lambda 2$ (e/bohr^5; black dotted line), and L (e/bohr^5; grey plain line) values for the S atom as a function of t, as obtained by comparing the *cm_lim* and *cm_fit* approaches.

To locate the CPs in progressively smoothed CM-based EDDs, the search algorithm illustrated by Equation 1 is applied from t = 0.00 to 5.00 bohr^2 with a Δt of 0.05 bohr^2. At t = 0 bohr^2, the model *cm_trunc* is selected with the original CM parameters (a_i, b_i) i = 1 to 4 only (Equation 5), while from t = 0.05 bohr^2, the model *cm_lim* is used. The refinement process expressed in Equation 1 stops when a lower limit $|\nabla\rho(\mathbf{r})|$ = 10^{-5} e/bohr^4 is reached.

Results and Discussion

a. Crystal structures

As already mentioned in the Introduction, four molecules belonging to the benzyl chalcocyanate series were selected (Figure 3). CIGGEE and NOTECN are isomorphous crystal structures[32] with, each, two short chalcogen…O distances, at 3.00 and 3.17, and 2.95 and 3.18 Å, respectively. The chalcogen…O network of CIGGII differs, as only one S…O interaction is characterized by a distance of 3.17 Å. In CIGGII, two other S…O contacts are present at distances of 3.59 and 3.72 Å. Chalcogen bonds correspond to the shortest chalcogen-O distances, i.e., below 3.2 Å [40,41]. In the structures CIGGII and CIGGOO, only one of such bonds is clearly identified, the second shortest distance being slighly longer than 3.5 Å, i.e., close to the sum over the van der Waals radius of the atoms.

In structures CIGGII and CIGGOO, each chalcogen atom is surrounded by a first layer of other chalcogen atoms located at a distance of 4.00 and 3.89 Å, respectively. The second layer of chalcogen atoms occurs at distances larger than 5 Å. In CIGGEE and NOTECN, the two chalcogen layers surrounding each chalcogen atom are located at distances of 4.74 and 4.75 Å, and 4.51 and 4.75 Å, respectively (Figure 3). For comparison purposes, two artificial crystal structures were built by substituing S by Se, and inversely, in structures CIGGII and CIGGEE. They are named CIGGII_Se and CIGGEE_S further in the text.

To analyze the BCPs involved in interactions with a molecule inside the crystal structure (further named the central molecule), we considered all atoms surrounding the central molecule at distances ≤ 8 Å. H atoms were introduced using the program Avogadro [42]. All BCPs included in a region limited by a lower and a larger bound of 0.8 and 2.8 Å from the central molecule were analyzed. The superimposition of the BCP positions along t provides the so-called BCP trajectory. To directly focus on the main intermolecular interactions, all analyses were carried out starting at the BCPs obtained from smoothed EDDs, at t = 1.5 bohr^2 [25].

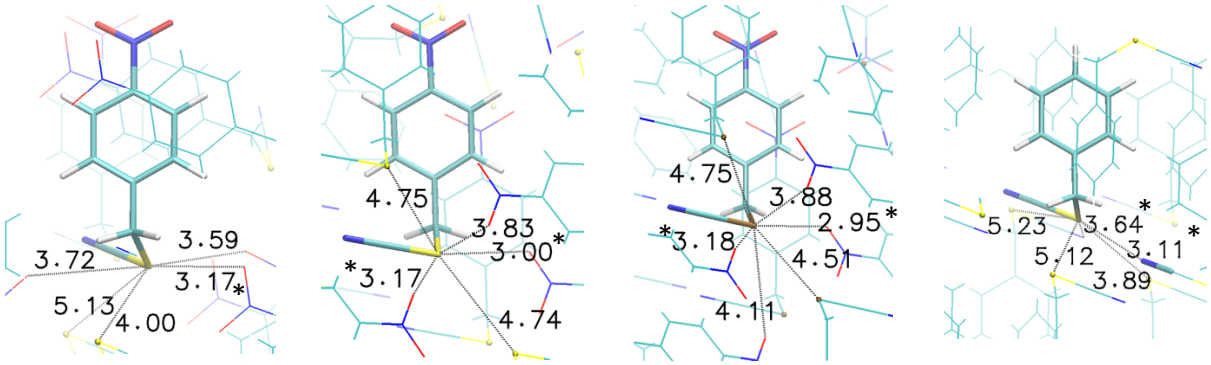

CIGGII (S) CIGGEE (Se) NOTECN (Te) CIGGOO (Se)

Figure 3. Crystal packing of the benzyl chalcocyanate derivatives with selected intermolecular chalcogen…O_{nitro} and chalcogen…chalcogen distances (in Å). (H = white, C = cyan, N = dark blue, O = red, S and Se = yellow, Te = brown). Chalcogen bonds are identified using (*).

b. Interactions with the chalcogen atoms

It is known that CPs always annihilate with the scale [43]. The number of CPs is thus reduced when t increases [25]. At t < 0.1 bohr^2, all atoms, including the H atoms, are seen as density maxima

(peaks). At $t = 0.1$ bohr^2, the H atoms are not detected any longer. Around $t = 1.5$ bohr^2, the number of density peaks is reduced so that there remain three to four peaks per molecule, one on the NO_2 group, one on the chalcogen atom, and one to two peaks at the level of the aromatic ring. In CIGGOO, there is one peak less due to the absence of the nitro group, while in NOTECN, there is one peak less in the ring due to the large size of the Te atom. At about $t = 2.0$ bohr^2, three peaks (or less for CIGGOO and NOTECN) can be assigned to each molecule (NO_2 group, chalcogen atom, aromatic ring), and at $t = 3.0$ bohr^2, only two peaks remain for each molecule, in the vicinity of the nitro and chalcogen atoms. Thus, smoothed EDDs appear to depict medium or low resolution maps. It has been shown that for proteins, EDDs show similar shapes at $t = 0.45$ bohr^2 and resolution $d = 2$ Å , at $t = 0.8$ bohr^2 and $d = 2.5$ Å, and at $t = 1.5$ bohr^2 and $d = 3$ Å [39].

In the unsmoothed EDD, BCPs are well aligned with their two closest atoms, i.e., either two oxygen atoms of the surrounding nitro groups or, in CIGGOO, two nitrogen atoms of the cyano groups. They actually correspond to the interactions identified by Maartmann-Moe et al. [32] in the crystal structures CIGGII, CIGGEE, NOTECN, and CIGGOO, and encompass the chalcogen bonds. Additional chalcogen…BCP…O motifs observed in the nitrobenzyl chalcocyanate compounds correspond to the longest chalcogen…O/N distances and are not perfectly linear. When the smoothing degree is significantly larger than zero, good alignements are observed between a BCP and two more distant atoms.

A description of the BCPs involving the chalcogen atoms is reported in Table 1, in terms of trajectory length $[t_i\text{-}t_f]$, atom…atom distance, and occurrrence of a RDG minimum. Due to the crystal environment, a BCP associated with an *atom1* of the central molecule and an *atom2* of a neighboring molecule has an image located between *atom2* of the central molecule and *atom1* of a neighboring molecule. Table 1 reports data for one image only.

c. Chalcogen…nitro and chalcogen…cyano bond critical points

As mentioned above, the chalcogen…nitro BCPs appear at the shortest corresponding intermolecular distances. They mainly involve O atoms of the nitro groups, but some of them involve the nitrogen of a nitro group (Table 1, Figure 4). In CIGGII, three of such BCPs are observed at $t = 0$ bohr^2 (inversely, three BCPs are observed between the nitro group of the central molecule and neighboring chalcogen atoms). They initiate BCP trajectories, with t_f end values that are inversely correlated with the distance S…O/N. Precisely, the *distance*-t_f pairs are (3.17, 5),

(3.72, 3), and (4.35 Å, 1.9 bohr^2). In CIGGEE_S, where the crystal parameters are too large for the S-containing compound, all BCP trajectories exist up to t = 5 bohr^2, while only one BCP of CIGGII is part of a complete trajectory. In contrast, in CIGGEE that originally contains Se, all three BCP trajectories end before t = 3.7 bohr^2 and, likely due to steric constraints, a BCP trajectory of CIGGII_Se ends prematurately at t_f = 1.8 bohr^2.

Five chalcogen…nitro BCP trajectories with the most negative L values, i.e., the highest local ED concentration, characterize each a BCP involved in a chalcogen bond, i.e., CIGGII ($d_{S\text{-}O}$ = 3.17 Å), CIGGEE_S ($d_{S\text{-}O}$ = 3.00 Å), CIGGEE ($d_{Se\text{-}O}$ = 3.00 Å), and NOTECN ($d_{Te\text{-}O}$ = 2.95 Å), as well as the BCP of CIGGII_Se with a Se…O distance of 3.17 Å (Figure 5). The three most negative, but also the three shortest, profiles are associated with the heaviest chalcogen atoms Se and Te.

The ellipticity profiles reported in Figure 5 show that the BCPs undergo a drastic flattening of the local EDD right before annihilation. The moderate increase of ε in the third BCP trajectory of CIGGEE_S suggests that the annihilation of that BCP is expected to appear soon after t = 5 bohr^2, while the three other complete trajectories tend to exist longer after t = 5 bohr^2.

Table 1. BCPs involved in the chalcogen-dependent interactions with the corresponding chalcogen…atom distance *(A: d)*, where *A* and *d* stand for the atom type and the distance value (Å), respectively. [t_i-t_f]-t_s is the trajectory length involving the BCP (bohr^2) followed by the t_s value (in italic) at which a RDG minimum is observed (bohr^2). Trajectories up to t = 5 bohr^2 are noted in bold.

	chalc…nitro	chalc…chalc	chalc…arom
S compounds			
CIGGII	**[0.0-5.0] (O: 3.17)** [0.0-3.0]-*3.1* (O: 3.72) [0.0-1.9] (O : 3.59)	**Two trajectories [0.0-5.0]** Coalescence at t = 0.9 (S: 4.00) [a-0.9] **[0.0-5.0] (S: 5.13)** [a-1.9]	/
CIGGEE_S	**[0.0-5.0] (O: 3.00)** **[0.0-5.0] (O: 3.17)** **[0.0-5.0] (N: 3.80)**	[0.0-0.0] (S: 4.74)	/
Se compounds			
CIGGEE	[0.0-3.3] (O: 3.00) [0.0-3.6] (O: 3.17) [0.0-3.4]-*3.5* (N: 3.80, O:3.83)	**[0.0-5.0] (Se: 4.75)** [b] **[0.0-5.0] (Se: 4.75)** [a-3.0, b] **[1.6-5.0] (Se: 4.74)** [a-2.6]	[0.0-1.6] (C: 4.16)

CIGGII_Se	[0.0-3.5] (O: 3.59) [0.0-3.3] (O: 3.17) [0.0-1.8] (O: 3.72)	**Two trajectories [0.0-5.0]** Coalescence at t = 1.9 (Se: 5.13) [a-1.9] **[0.0-5.0] (Se: 4.00)** [a-0.0]	/
CIGGOO	/	**Two trajectories [0.0-5.0]** Coalescence at t = 1.5 (Se: 5.12) [a-1.5] **Two trajectories [0.0-5.0]** Coalescence at t = 2.2 (Se: 5.23) [a-2.2] **[0.0-5.0] (Se: 3.89)** [a-0.0]	**[0.0-5.0] (C: 4.03)** [b] [0.0-2.5]-*2.6* (C: 4.02) [b]
Te compound			
NOTECN	[0.0-2.4] (O: 2.95) [0.0-2.4]-*2.5* (O: 3.18) [0.0-2.5]-*2.6* (N: 3.85) [0.0-1.6]-*1.7* (O: 4.11)	**[0.0-5.0] (Te: 4.51)** [a-0.0] **[1.7-5.0] (Te: 4.75)** **[1.6-5.0] (Te: 4.75)**	/

[a-t] immobile BCP from the mentioned value of t

[b] not perfectly in the alignment of two chalcogen atoms at t = 1.5 bohr^2

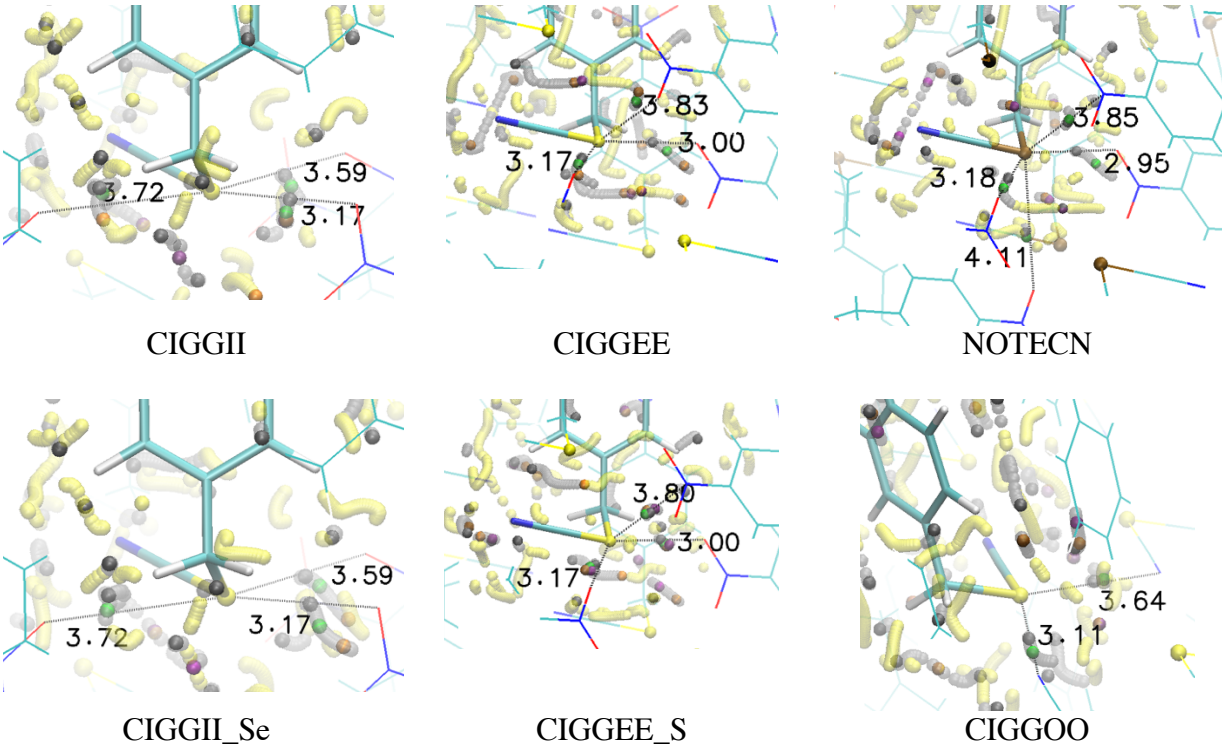

Figure 4. BCPs at t = 1.5 bohr^2 depicting the chalcogen…nitro and the chalcogen…N_{cyano} interactions in CIGGOO (green spheres), BCP (pale yellow spheres), and RCP (pale grey spheres) trajectories. BCPs at t = 0.0, 3.0, and 4.5 bohr^2 are shown in black, orange, and purple, respectively. Distances are in Å.

It was observed that chalcogen-nitro BCP trajectories that terminate before $t = 5$ bohr^2 meet a RCP trajectory and further yield a RDG minimum. It is especially clear for the NOTECN structure (Figure 6, Table 1). Most of the RDG minima are characterized by negative values of $\lambda 2$, but all have an extremely low value of $s(\boldsymbol{r})$, consistently with the original value of $s(\boldsymbol{r}) = 0$ for a CP. The merge of trajectories of different types explains the decrease in the number of CPs as t increases [43]. RDG minima are also found at the end of single CP trajectories (Figure 6).

The absence of nitro groups in CIGGOO leads to two chalcogen…N_{cyano} BCPs ($d_{Se\text{-}N} = 3.11$ and 3.64 Å) which are observed only in that particular structure (Figure 4). Their trajectory starts at $t = 0$ bohr^2 and ends at $t_f = 2.7$ and 2.1 bohr^2, respectively. They correspond to the two interactions originally detected by Maartmann-Moe et al. [32] The corresponding Laplacian profiles show a minimum between 1.8 and 2.0 bohr^2, and the ellipticity increases just before annihilation (Figure SI2).

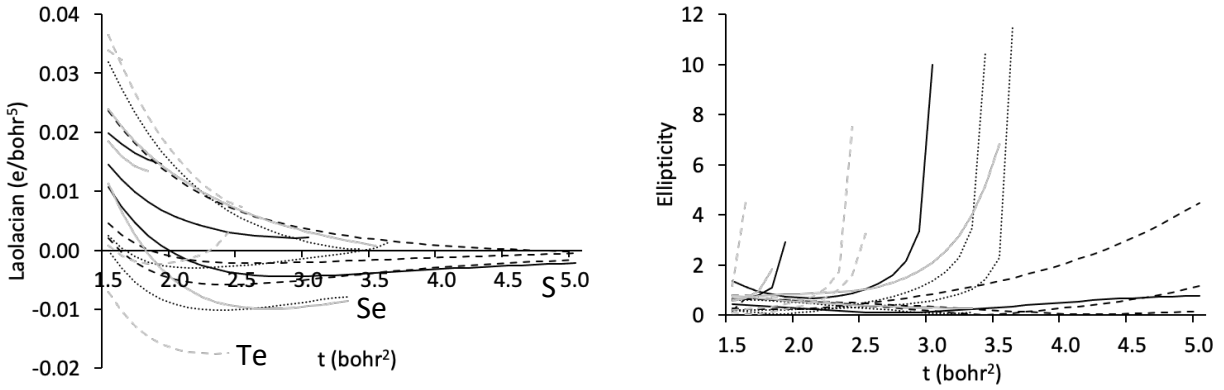

Figure 5. Profile of the Laplacian and ellipticity as a function of t for the BCP trajectories involved in a chalcogen…nitro interaction (CIGGII: plain black, CIGGEE_S: dashed black, CIGGEE: dotted black, CIGGII_Se: plain grey, NOTECN: dashed grey).

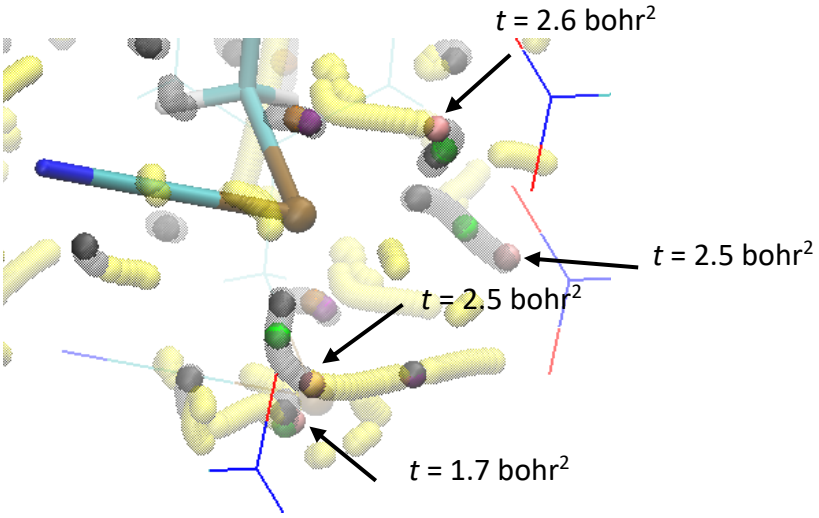

Figure 6. BCPs at t = 1.5 bohr² (green spheres) depicting the chalcogen…nitro interactions in NOTECN, BCP (pale yellow spheres), and RCP (pale grey spheres). BCPs at t = 0.0, 3.0, and 4.5 bohr² are shown in black, orange, and purple, respectively. RDG minima at t = 1.7, 2.5, and 2.6 bohr² are shown with pink spheres and arrows.

d. Chalcogen…chalcogen bond critical points

In the unsmoothed EDDs, the BCPs that are associated with that family of interactions are not perfectly aligned with two neighboring chalcogen atoms. They become linearly placed at about t = 3 bohr², and they are all present until t = 5 bohr², except in the artificial structure CIGGEE_S wherein no clear chalcogen…chalcogen BCP is detected. Actually, beyond t = 3 bohr², all detected BCPs are chalcogen…chalcogen ones, except for the S-containing structures, i.e., CIGGII and CIGGEE_S, wherein S is not large enough to mask other interactions such as, e.g., the S…nitro and nitro…nitro ones.

In the isomorphous crystal structures CIGGEE and NOTECN, several chalcogen…chalcogen BCPs belong to trajectories that begin after t = 0 bohr². This is not observed in the S-containing structures. After a short smoothing stage, the Se and Te EDD mask the EDD of the cyano groups when the chalcogen…chalcogen separation distances are $\leq$ 4.75 Å. In CIGGII, one of the BCP depicts a chalcogen…chalcogen interaction only after t = 0.9 bohr². Its location actually results from the merge of two BCP trajectories that begin at the level of two H_2C…chalcogen mid-distances to yield a single BCP that stays immobile from t = 0.9 to 5.0 bohr² (Table 1, Figure 7). A second chalcogen…chalcogen BCP is linearly placed between its two neighboring chalcogen atoms at $t \geq$ 1.9 bohr². A number of chalcogen…chalcogen BCP

trajectories are initially located between two close H_2C-chalcogen or cyano-chalcogen chemical bonds and eventually end to form linear chalcogen…BCP…chalcogen patterns. In contrast, many chalcogen…chalcogen BCPs, whose trajectory starts at $t = 0$ bohr^2, are immobile after some value of t. It is observed in the structures containing the largest chalcogen atom, Se or Te, i.e., in CIGGEE, CIGGOO, CIGGII_Se, and NOTECN, but also in CIGGII with a peculiar BCP behavior for the longest S…S distance of 5.13 Å (Table 1). In NOTECN, three BCPs are associated with chalcogen…chalcogen interactions. Those BCPs are aligned with their chalcogen neighbors only from $t = 3$ bohr^2 except for the immobile BCP associated with the shortest Te…Te distance of 4.51 Å (Figure 7).

In CIGGEE_S, despite the presence of a S…BCP…S alignment in the unsmoothed EDD, no linear S…BCP…S patterns are observed at $t = 1.5$ bohr^2. It could explain the natural crystallization arrangement CIGGII versus CIGGEE_S. In CIGGII_Se, the other artificial structure considered, only two linear Se…BCP…Se arrangements are detected, compared to the original Se-based structure CIGGEE which involves three of such arrangements. One is already present from $t = 0$ bohr^2 along the shortest Se…Se separation distance of 4.0 Å, the other is fully established at $t = 2.0$ bohr^2, at the longest separation distance of 5.13 Å. It results from the merge of two BCP trajectories starting at the level of the two Se…cyano separation vectors ($d_{Se\text{-}N} = 3.55$ Å). At $t = 4.5$ bohr^2, the number of chalcogen…chalcogen BCPs is maximized compared to the artificial structures, i.e., two BCPs in CIGGEE versus none in CIGGEE_S, and three BCPs in CIGGII versus two in CIGGII_Se. Finally, the CIGGOO structure is the only one to show complete BCP trajectories (from 0 to 5 bohr^2) associated with three Se…Se interactions (Table 1). One BCP remains immobile and is linearly placed between the two closest Se atoms ($d_{Se\text{-}Se} = 3.89$ Å), while the two others result from the merge of two trajectories starting either between two parallel Se…CH_2 ($d_{Se\text{-}C} = 4.08$ Å) or two Se…cyano ($d_{Se\text{-}N} = 3.64$ Å) vectors, and are seen at Se…Se separation distances of 5.12 and 5.23 Å (Figure 7). These two last BCPs actually stay located at central positions between two facing H_2C-Se bonds and two Se-cyano bonds from $t = 1.5$ and 2.2 bohr^2, respectively. A peculiarity of the NOTECN structure is the absence of any central Te-cyano…cyano-Te BCP compared to the other five structures. Indeed, Te is so large that it rapidly masks the EDD of the other atoms as t increases.

At $t = 1.5$ bohr^2, all intermolecular BCPs are characterized by $L > 0$ (Figure 8). Above $t = 2.5$ bohr^2, the intermolecular region is progressively enriched in ED versus the intramolecular

regions, and thus shows negative values of L [25]. At $t > 4.5$ bohr^2, all chalcogen…chalcogen BCPs are eventually characterized by $L < 0$, except for the BCP appearing at $t = 1.6$ bohr^2 in CIGGEE. Figure 8 also shows discontinuities along the L profiles of a BCP in CIGGOO and CIGGII_Se, each occurring at the coalescence of two BCPs trajectories at $t = 2.2$ and 1.9 bohr^2, respectively (Table 1). Such L discontinuities correspond to a maximum in the ellipticity profiles. However, a maximum in an ellipticity profile does not necessarily correspond to a discontinuity in L, as illustrated in Figure 8 for the second BCP of the CIGGII system which adopts the linear S…BCP…S pattern starting at $t = 1.9$ bohr^2.

e. Chalcogen…aromatic ring bond critical points

Chalcogen…aromatic interactions are observed, to a limited extend only, in the Se-containing structures CIGGEE and CIGGOO (Table 1). In the nitro-containing structure CIGGEE, the single BCP trajectory ends at $t_f = 1.6$ bohr^2, while in CIGGOO, the two BCP trajectories are longer, i.e., they end at $t = 2.5$ and 5.0 bohr^2. They are likely favored by the absence of nitro groups. The longest trajectory starts between Se and an aromatic ring, and eventually moves to a H_2C…aromatic type interaction. The L and ε profiles suggest that the longest BCP trajectory of CIGGOO is expected to last after $t = 5$ bohr^2 (Figure SI3).

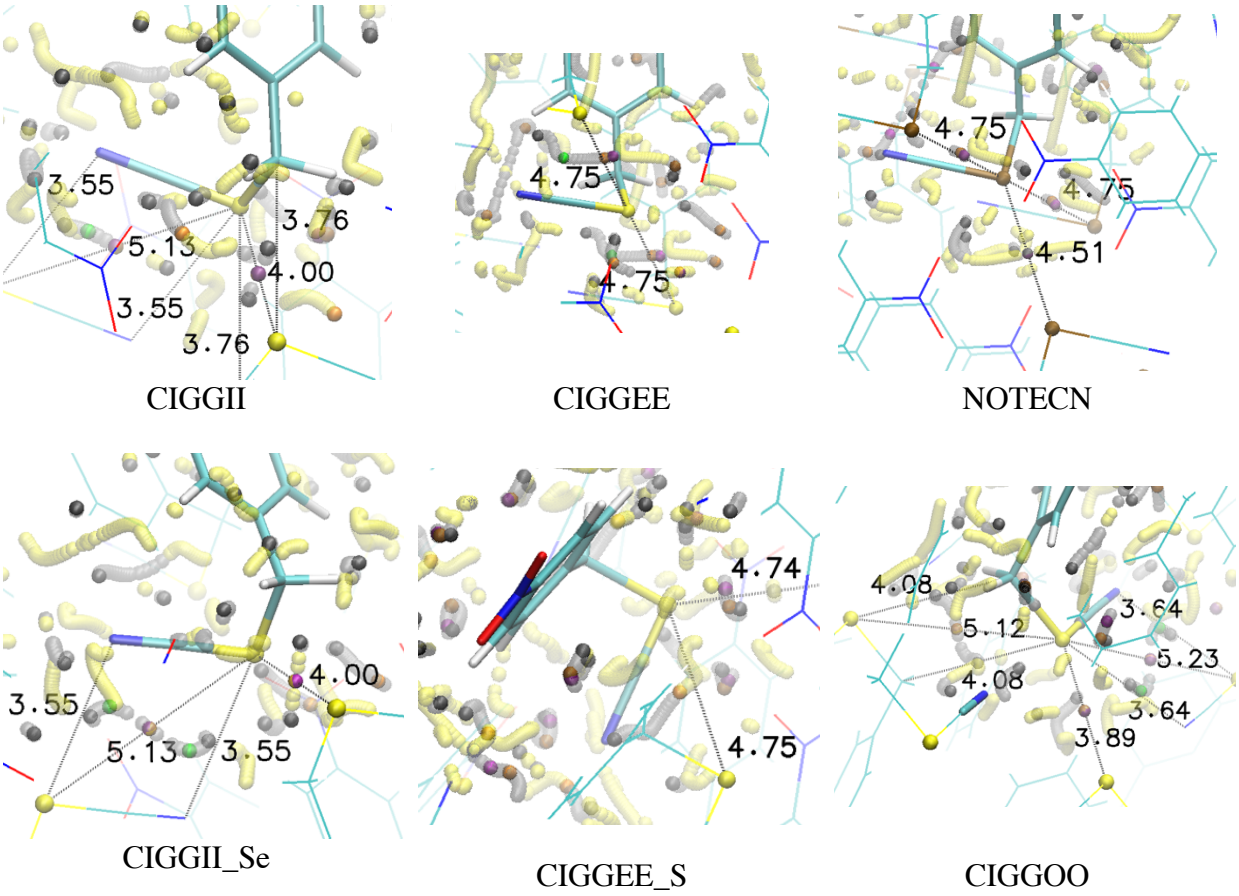

Figure 7. BCPs at t = 1.5 and 3.0 bohr^2 depicting the chalcogen…chalcogen interactions (green and orange spheres, respectively), BCP (pale yellow spheres), and RCP (pale grey spheres) trajectories. BCPs at t = 0.0 and 4.5 bohr^2 are shown with black and purple spheres, respectively. Distances are in Å.

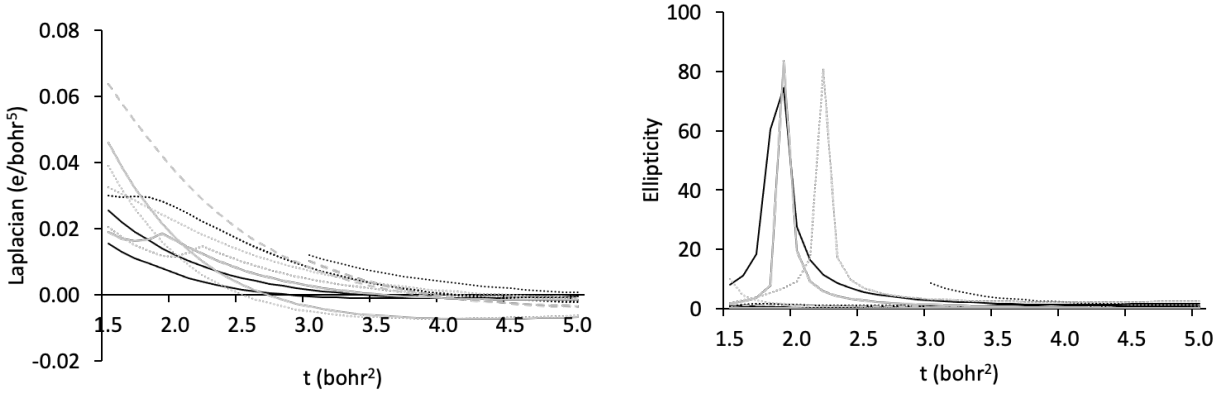

Figure 8. Profile of the Laplacian and ellipticity as a function of *t* for the BCP trajectories depicting a chalcogen…chalcogen interaction (CIGGII: plain black, CIGGEE: dotted black, CIGGII_Se: plain grey, CIGGOO: dotted grey, NOTECN: dashed grey).

f. Nitro group…aromatic ring bond critical points

Besides chalcogen…nitro BCPs, nitro…aromatic ring interactions are detected in all structures with a nitro group (Table 2, Figure SI4). The BCP trajectories remain confined in a limited area between the nitro group and the aromatic cycle of the central molecule, in a region of low ED ρ. In the three structures containing the heaviest Se and Te, the BCP trajectory terminates by a RDG minimum at the meeting point with a RCP trajectory, while in the two S-based compounds, there is no RCPs in the direct vicinity of the BCP trajectories. One also notices slight discrepancies between BCP trajectories and their symmetry image, e.g., in CIGGEE, the trajectory lengths are characterized by [0.0-3.6] and [0.1-3.5] bohr^2. Such interactions are likely to be less precisely located due to extremely low ρ values and flat EDDs.

As the atomic number of the chalcogen atom increases, the BCP trajectories end at decreasing values of t_f (Table 2). Particularly, t_f is at least equal to 5 bohr^2 for S-containing structures. It is due to the fact that the EDD shape is guided by the molecular skeleton up to a progressively larger t_f value, before being oriented along the chalcogen atom crystal rows (Figure SI5). In the case of CIGGII-based structures, the N_{nitro} is almost directly facing a carbon atom of an aromatic ring (N_{nitro}…C_{arom} distance = 3.54 Å). In the other structures, N_{nitro} is facing the aromatic ring region which is ED-depleted.

Except for CIGGEE, all L values are negative at t = 3.5 bohr^2 and beyond, depicting a concentration in the ED (Figure SI6). Regardless of the different t_f values, the L profiles are evolving similarly whatever the nature of the chalcogen atom; it is consistent with the position of the BCPs away from the chalcogen locations. As already observed earlier, the ellipticity profiles show an abrupt increase at the annihilation t, or smoothly increase for the persistent BCPs.

A number of other types of BCPs involving the nitro or the cyano groups of the considered chalcocyanate crystals, as well as the aromatic rings, have also been identified. For completeness, they are all reported in the Supplementary Information section of the paper (Table SI1).

Table 2. BCPs involved in the nitro…aromatic interactions; $[t_i\text{-}t_f]\text{-}t_s$ is the trajectory length involving the BCP (bohr^2) followed by the t_s value (in italic) at which a RDG minimum is observed (bohr^2). Trajectories up to t = 5 bohr^2 are noted in bold.

		$[t_i\text{-}t_f]\text{-}t_s$
S compounds	CIGGII	**[0.7-5.0]**
	CIGGEE_S	**[0.0-5.0]**
Se compounds	CIGGEE	[0.0-3.6]-*3.7*
	CIGGII_Se	[1.1-4.2]-*4.3*
Te compound	NOTECN	[0.0-2.8]-*2.9*

Conclusions and perspectives

A study of intermolecular interactions, based on the critical point (CP) analysis of promolecular Cromer-Mann (CM) electron density distribution (EDD) functions at different smoothing degrees, is applied to several crystal systems involving chalcogen bonds. The approach allows the visualization of the trajectories of the bond and ring CPs (BCPs and RCPs) along the smoothing factor t. The interactions are described in terms of their trajectory length and the presence of a Reduced Density Gradient (RDG) minimum. The Cromer-Mann EDDs, analytically constructed from tabulated parameters, provide an enriched set of interactions compared to an atom…atom distance analysis. The search for CPs is fast and does not require any grid calculations.

Smoothing the EDD is a procedure that allows to preserve the number of electrons and to mimick the effect of temperature to some extent. Smoothing leads to a progressive loss of details as also observed experimentally following a change in the crystallographic resolution, e.g., t = 1.5

bohr^2 leads to similar EDD shape as at a resolution of 3 Å. Working with smoothed EDD allows to focus on a limited set of significant interaction types, herein especially the chalcogen-based interactions. Interestingly, it unveils interactions during the progress of the EDD smoothing.

Within the selected benzyl chalcocyano structures (CSD codes CIGGII, CIGGEE, NOTECN, and CIGGOO), several kinds and number of interactions are observed, depending upon the type of chalcogen atom, the presence of a nitro group, and the smoothing level.

In the unsmoothed EDDs, i.e., at t = 0.0 bohr^2, the chalcogen bonds appear as linear chalcogen…BCP…O/N patterns, with the most negative Laplacian values at the BCP locations. The BCP trajectories end at progressively lower values of t_f as the atomic number increases. In the absence of a nitro group, i.e., in CIGGOO, other linear patterns are observed for the chalcogen…BCP…aromatic and chalcogen…BCP…N_{cyano} interactions, the latter corresponding to chalcogen bonds. At t = 1.5 bohr^2, other linear chalcogen…BCP…nitro patterns are observed with trajectories ending below t_f = 5 bohr^2 as for the chalcogen bonds. At a value of t = 3.0 bohr^2, linear chalcogen…BCP…chalcogen patterns are unveiled. They are the only observable interactions left, except for the S-containing compounds wherein S is not large enough to mask other types of interactions. Several chalcogen…chalcogen BCPs actually originate from the coalescence of two BCP trajectories. Once the coalescence is achieved, the BCP remains immobile with t. The number of chalcogen…chalcogen BCPs is reduced in the artificial structures built by exchanging S with Se, compared to the original crystal arrangements.

The merge of a BCP and a RCP trajectories leads to the occurrence of a minimum in the reduced density gradient (RDG) distribution. Such phenomenon is more likely to occur in the Se and Te-containing structures. It suggests that specific interactions, such as chalcogen…nitro, nitro…aromatic, cyano…aromatic, and aromatic…aromatic, can subsist as weak interactions after the disappearance of their corresponding BCP. The occurrrence of RDG minima is also observed at the termination of single BCP and RCP trajectories, showing a progressive weakening of the corresponding interactions.

Non-covalent interactions (NCIs), and their strength, are generally analyzed from (QM) ED maps [44]. To evaluate the evolution of the CPs in QM ED maps at various levels of details, it is suggested that smoothing of the ED maps could be achieved through numerical techniques such as wavelet multiresolution analysis [45] or convolution neural networks [46], as instances. Another

approach consists in using a database of QM aspherical structure factors, such as in the Invariom refinement method [47,48], from which EDDs could be reconstructed at different levels of resolution. The assignment of an energy-related descriptor to the BCPs found in smoothed EDDs can also lead to the evaluation of the interaction competitiveness. Such an energy descriptor has already been proposed to assess hydrogen bonds in QM and experimental ED maps [49]. It is based on the density and Laplacian values at the BCP locations. Despite the questionning about its validity [50], it is considered as a starting point for an energy-based classification of the BCPs. The evaluation of the energetics of NCIs can also be carried out by integrating selected properties inside low-value RDG isocontours [51].

Acknowledgments

The authors gratefully thank the Reviewers for their useful comments and suggestions. The present research used resources of the 'Plateforme Technologique de Calcul Intensif (PTCI)' (http://www.ptci.unamur.be) located at the University of Namur, Belgium, which is supported by the FNRS-FRFC under the conventions No. 2.5020.11. The PTCI is member of the 'Consortium des Équipements de Calcul Intensif (CÉCI)' (http://www.ceci-hpc.be), funded by the 'Fonds de la Recherche Scientifique de Belgique (F.R.S.-FNRS)'.

References

[1] Bader R F W 1994 *Atoms in molecules: A quantum theory*. Oxford University Press: Oxford

[2] Contreras-García J, Yang W, Johnson E R 2011 Analysis of hydrogen-bond interaction potentials from the electron density: Integration of noncovalent interaction regions *J. Phys. Chem. A* **115** 12983–12990

[3] Narth C, Maroun Z, Boto R A, Chaudret R, Bonnet M-L, Piquemal J-P, Contreras-García J 2016 A complete NCI perspective: From new bonds to reactivity. In *Applications of topological methods in molecular chemistry*. Chauvin R, Lepetit C, Silvi B, Alikhani E (Eds) Springer: Cham, 491–527

[4] Bauzá A, Frontera A 2020 Halogen and chalcogen bond energies evaluated using electron density properties *ChemPhysChem* **21** 26–31

[5] Scheiner S 2019 Forty years of progress in the study of the hydrogen bond *Struct. Chem.* **30** 1119–1128

[6] De Silva V, Averkiev B B, Sinha A S, Aakeröy C B 2021 The balance between hydrogen bonds, halogen bonds, and chalcogen bonds in the crystal structures of a series of 1,3,4-chalcogenadiazoles *Molecules* **26** 4125

[7] Tsirelson V G, Avilov A S, Abramov Y A, Belokoneva E L, Kitaneh R, Feil D 1998 X-ray and electron diffraction study of MgO *Acta Crystallogr. B* **54** 8–17

[8] Downs R T, Gibbs G V, Boisen Jr M B, Rosso K M 2002 A comparison of procrystal and ab initio model representations of the electron-density distributions of minerals *Phys. Chem. Miner.* **29** 369–385

[9] Bultinck P, Carbó-Dorca R, Van Alsenoy C 2003 Quality of approximate electron densities and internal consistency of molecular alignment algorithms in molecular quantum similarity *J. Chem. Inf. Comput. Sci.* **43** 1208–1217

[10] Bouhmaida N, Ghermani N E 2005 Elusive contribution of the experimental surface molecular electrostatic potential and promolecule approximation in the empirical estimate of the crystal density *J. Chem. Phys.* **122** 114101

[11] Bentley J 1998 Behavior of electron density functions in molecular interactions *J. Phys. Chem. A* **102** 6043–6051

[12] Mitchell A, Spackman M 2000 Molecular surfaces from the promolecule: A comparison with Hartree–Fock ab initio electron density surfaces *J. Comput. Chem.* **21** 933-942

[13] Spackman M A 2006 The use of the promolecular charge density to approximate the penetration contribution to intermolecular electrostatic energies *Chem. Phys. Lett.* **418** 158–162

[14] Keyvani Z A, Shahbazian S, Zahedi M 2016 To what extent are "atoms in molecules" structures of hydrocarbons reproducible from the promolecule electron densities? *Chem. – Eur. J.* **22** 5003–5009

[15] Jabłoński M 2019 Bond paths between distant atoms do not necessarily indicate dominant interactions *J. Comput. Chem.* **39** 2183–2195

[16] Taylor R 2020 Identifying intermolecular atom···atom interactions that are not just bonding but also competitive *CrystEngComm* **22** 7145–7151

[17] Tsirelson V G, Abramov Y U A, Zavodnik V E, Stash A I, Belokoneva E L, Stahn J, Pietsch U, Feil D 1998 Critical points in a crystal and procrystal *Struct. Chem.* **9** 249–254

[18] Saleh G, Gatti C, Lo Presti L 2012 Non-covalent interaction via the reduced density gradient: Independent atom model vs experimental multipolar electron densities *Comput. Theor. Chem.* **998** 148–163

[19] Genoni A, Bučinský L, Claiser N, Contreras-García J, Dittrich B, Dominiak P M, Espinosa E, Gatti C, Giannozzi P, Gillet J, Jayatilaka D, Macchi P, Madsen A Ø, Massa L, Matta C F, Merz K M, Nakashima P N H, Ott H, Ryde U, Schwarz K, Sierka M, Grabowsky S 2018 Quantum crystallography: Current developments and future perspectives *Chem. – Eur. J.* **24** 10881–10905

[20] Massa L, Matta C F 2018 Exploiting the full quantum crystallography *Can. J. Chem.* **96** 599-605

[21] De Bruyne B, Gillet J-M 2020 Inferring the one-electron reduced density matrix of molecular crystals from experimental data sets through semidefinite programming *Acta Crystallogr. A* **76** 1–6

[22] Bader R F W, Matta C F 2001 Bonding to Titanium *Inorg. Chem.* **40** 5603–5611

[23] Matta C F, Hernández-Trujillo J, Tang T-H, Bader R F W 2003 Hydrogen–hydrogen bonding: A stabilizing interaction in molecules and crystals *Chem. - Eur. J.* **9** 1940–1951

[24] Girones X, Amat L, Carbó-Dorca R 2002 Modeling large macromolecular structures using promolecular densities *J. Chem. Inf. Comput. Sci.* **42** 847–852

[25] Leherte L 2021 Multiresolution non-covalent interaction analysis for ligand–protein promolecular electron density distributions *Theor. Chem. Acc.* **140** 9

[26] Leherte L 2021 Correction to: Multiresolution non-covalent interaction analysis for ligand–protein promolecular electron density distributions *Theor. Chem. Acc.* **140** 88

[27] Good A C, Hodgkin E E, Richards W G 1992 Utilization of Gaussian functions for the rapid evaluation of molecular similarity *J. Chem. Inf. Comput. Sci.* **32** 188–191

[28] Maggiora G M, Rohrer D C, Mestres J 2001 Comparing protein structures: A Gaussian-based approach to the three-dimensional structural similarity of proteins *J. Mol. Graph. Model.* **19** 168–178

[29] Kostrowicki J, Piela L, Cherayil B J, Scheraga H A 1991 Performance of the diffusion equation method in searches for optimum structures of clusters of Lennard-Jones atoms *J. Phys. Chem.* **95** 4113–4119

[30] Duncan B S, Olson A J 1993 Shape analysis of molecular surfaces *Biopolymers* **33** 231–238

[31] Brown P J, Fox A G, Maslen E N, O'Keefe M A, Willis B T M 2006 Intensity of diffracted intensities. In *International Tables for Crystallography Volume C*. Prince E (Ed) Springer: Dordrecht 554–595

[32] Maartmann-Moe K, Sanderud K A, Songstad J, Sillanpää R, Fernholt L, Rømming C 1984 The crystal structure of 4-nitrobenzyl tellurocyanate, 4-nitrobenzyl selenocyanate, 4-nitrobenzyl thiocyanate and benzyl selenocyanate *Acta Chem. Scand.* **38a** 187–200

[33] Scilabra P, Terraneo G, Resnati G 2019 The chalcogen bond in crystalline solids: A world parallel to halogen bond *Acc. Chem. Res.* **52** 1313–1324

[34] Shahbazian S 2018 Why bond critical points are not "bond" critical points *Chem. - Eur. J.* **24** 5401–5405

[35] Koritsanszky T S, Coppens P 2001 Chemical applications of X-ray charge-density analysis *Chem. Rev.* **101** 1583–1628

[36] Silva Lopez C, de Lera A R 2011 Bond ellipticity as a measure of electron delocalization in structure and reactivity *Curr. Org. Chem.* **15** 3576–3593

[37] Johnson E R, Keinan S, Mori-Sánchez P, Contreras-García J, Cohen A J, Yang W 2010 Revealing noncovalent interactions *J. Am. Chem. Soc.* **132** 6498–6506

[38] Boto R A, Contreras-García J, Tierny J, Piquemal J-P 2016 Interpretation of the reduced density gradient *Mol. Phys.* **114** 1406–1414

[39] Leherte L 2004 Hierarchical analysis of promolecular full electron-density distributions: Description of protein structure fragments *Acta Crystallogr. D* **60** 1254–1265

[40] Vogel L, Wonner P, Huber S M 2019 Chalcogen bonding: An overview *Angew. Chem. Int. Ed.* **58** 1880–1891

[41] Biot N, Bonifazi D 2020 Chalcogen-bond driven molecular recognition at work *Coord. Chem. Rev.* **413** 213243

[42] Hanwell M D, Curtis D E, Lonie D C, Vandermeersch T, Zurek E, Hutchison G R 2012 Avogadro: An advanced semantic chemical editor, visualization, and analysis Platform *J. Cheminformatics* **4** 17

[43] Kuijper A 2004 On detecting all saddle points in 2D images *Pattern Recognit. Lett.* **25** 1665–1672

[44] Scheiner S 2018 Comparison of various means of evaluating molecular electrostatic potentials for noncovalent Interactions *J. Comput. Chem.* **39** 500–510

[45] Starck J-L, Murtagh F, Bijaoui A 1998 *Image Processing and Data Analysis*. Cambridge University Press: Cambridge

[46] Jiang S, Zavala V M 2021 Convolutional neural nets in chemical engineering: Foundations, computations, and applications *AIChE J*. **67** e17282

[47] Dittrich B, Hübschle C B, Pröpper K, Dietrich F, Stolper T, Holstein J J 2013 The generalized invariom database (GID) *Acta Crystallogr. B* **69** 91–104

[48] Nelyubina Y V, Korlyukov A A, Lyssenko K A 2014 Probing weak intermolecular interactions by using the invariom approach: A comparative study of *s*-tetrazine *Chem. - Eur. J*. **20** 6978–6984

[49] Espinosa E, Molins E, Lecomte C 1998 Hydrogen bond strengths revealed by topological analyses of experimentally observed electron densities *Chem. Phys. Lett*. **285** 170–173

[50] Spackman M A 2015 How reliable are intermolecular interaction energies estimated from topological analysis of experimental electron densities? *Cryst. Growth Des*. **15** 5624–5628

[51] Saleh G, Gatti C, Lo Presti L 2015 Energetics of non-covalent interactions from electron and energy density distributions *Comput. Theor. Chem*. **1053** 53–59

Description of non-covalent interactions in benzyl chalcocyanate crystals from smoothed Cromer-Mann electron density distribution functions

Supplementary Information

Laurence Leherte, Laurie Bodart, Johan Wouters, Daniel P. Vercauteren

Laboratory of Structural Biological Chemistry, Unit of Theoretical and Structural Physical Chemistry, Department of Chemistry, NAmur Research Institute for LIfe Sciences (NARILIS), Namur Institute of Structured Matter (NISM), NAmur MEdicine & Drug Innovation Center (NAMEDIC), University of Namur, Rue de Bruxelles 61, B-5000 Namur (Belgium)

Email: laurence.leherte@unamur.be
ORCID: 0000-0001-8468-5462

The present research paper is our contribution in memory and honour of Enrico Clementi outstanding personality and prestigious career. LL and DPV have had the great chance to be invited by and collaborate with Enrico during numerous research stays particularly in Poughkeepsie, Kingston, Strasbourg, Cagliari, and Como. Among all our collaborations, one of his many ideas in his "Global simulation" scheme (cfr. notably in IJQC, 42, 547, 1992) concerned the importance of non-covalent interactions in solid state or life science systems, which we are tackling in the present work.

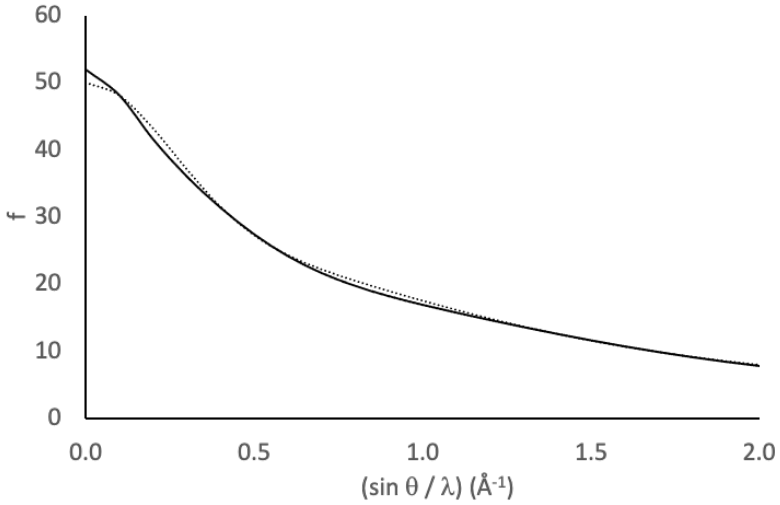

Figure SI1. Superimposition of the scattering factors of Te as obtained using the original CM coefficients (Equation 3, plain line) and using Equation 4 (dotted line). The fit was achieved using an ordinary least square approach, with analytical derivatives, applied to 400 values of *f* in the range 0 to 2.0 $Å^{-1}$.

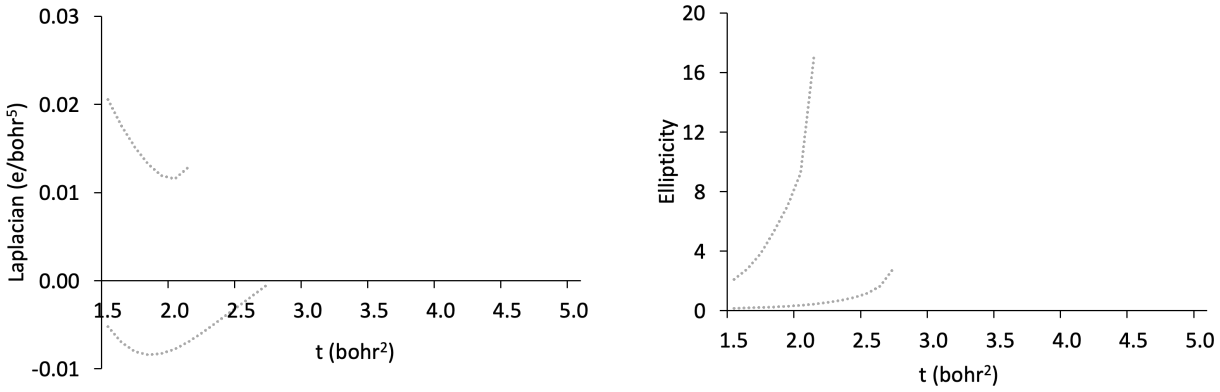

Figure SI2. Profile of the Laplacian and ellipticity as a function of *t* for the BCP trajectories of CIGGOO involved in the chalcogen…N_{cyano} interactions.

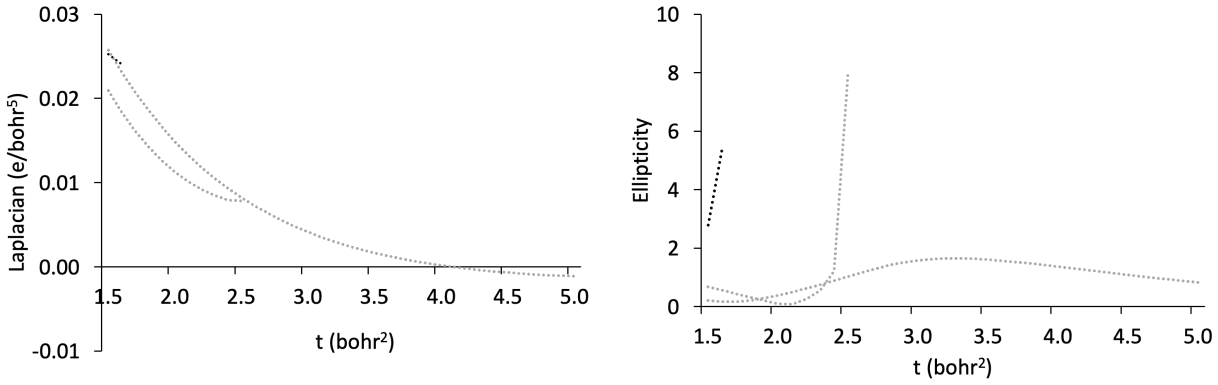

Figure SI3. Profile of the Laplacian and ellipticity as a function of *t* for the BCP trajectories involved in chalcogen…aromatic ring interactions (CIGGEE: dotted black, CIGGOO: dotted grey).

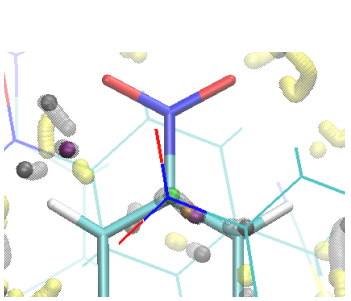

CIGGII

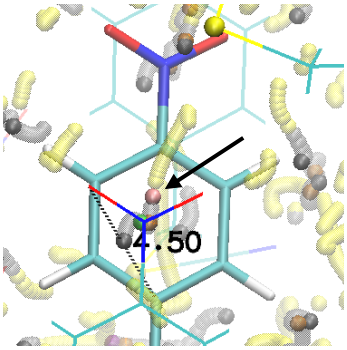

CIGGEE
RDG minimum @ 3.7 bohr²

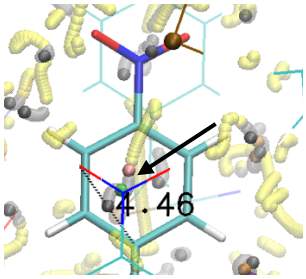

NOTECN
RDG minimum @ 2.9 bohr²

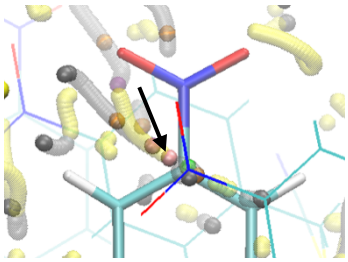

CIGGII_Se
RDG minimum @ 4.3 bohr²

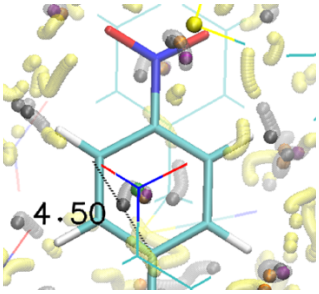

CIGGEE_S

Figure SI4. BCPs at $t = 1.5$ bohr² depicting the nitro…aromatic interactions (green spheres), BCP (pale yellow spheres), and RCP (pale grey spheres) trajectories. BCPs at $t = 0.0$, 3.0, and 4.5 bohr² are shown in black, orange, and purple, respectively. RDG minima observed between BCP and RCP trajectories are in pink (arrows).

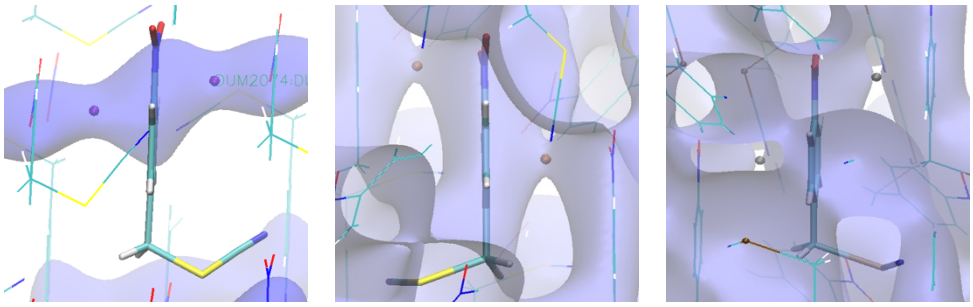

CIGGII	CIGGEE	NOTECN
t = 4.5 bohr^2	t = 3.0 bohr^2	t = 2.5 bohr^2
iso = 0.081 e/bohr^3	iso = 0.080 e/bohr^3	iso = 0.080 e/bohr^3

Figure SI5. Superimposition of the crystal structure, the ED iso-contour, and the nitro…aromatic BCPs (spheres) of CIGGII, CIGGEE, and NOTECN.

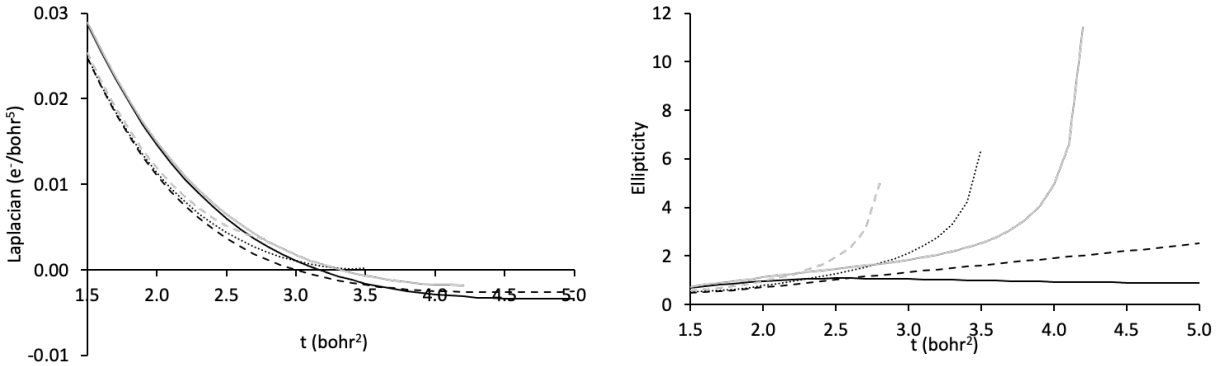

Figure SI6. Profiles of the Laplacian and ellipticity as a function of t for the BCP trajectories involved in the nitro…aromatic interactions (CIGGII: plain black, CIGGEE_S: dashed black, CIGGEE: dotted black, CIGGII_Se: plain grey, NOTECN: dashed grey).

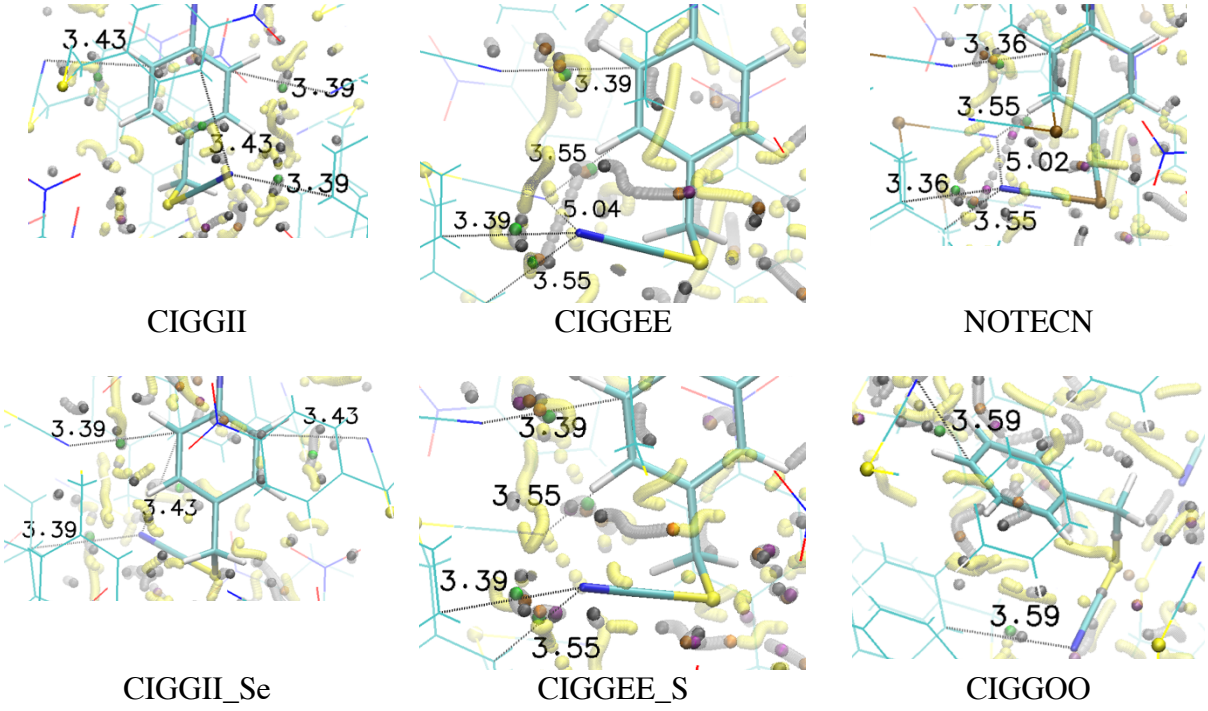

CIGGII CIGGEE NOTECN

CIGGII_Se CIGGEE_S CIGGOO

Figure SI7. BCPs at t = 1.5 bohr^2 depicting the N_{cyano}…arom interactions (green spheres), BCP (pale yellow spheres), and RCP (pale grey spheres) trajectories. BCPs at t = 0.0, 3.0, and 4.5 bohr^2 are shown in black, orange, and purple, respectively. Distances are in Å.

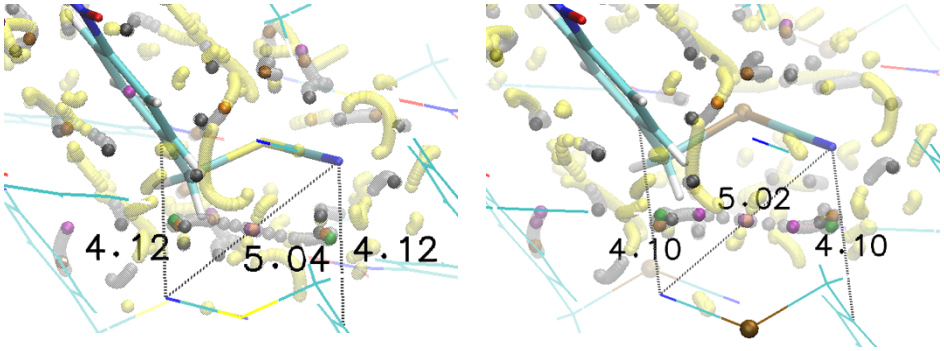

CIGGEE NOTECN

Figure SI8. BCPs depicting the transformation of the N_{cyano}…arom to N_{cyano}…N_{cyano} interactions, BCP (pale yellow spheres), and RCP (pale grey spheres) trajectories. BCPs at t = 0.0, 1.5, 3.0, and 4.5 bohr^2 are shown in black, green, orange, and purple, respectively. Distances are in Å.

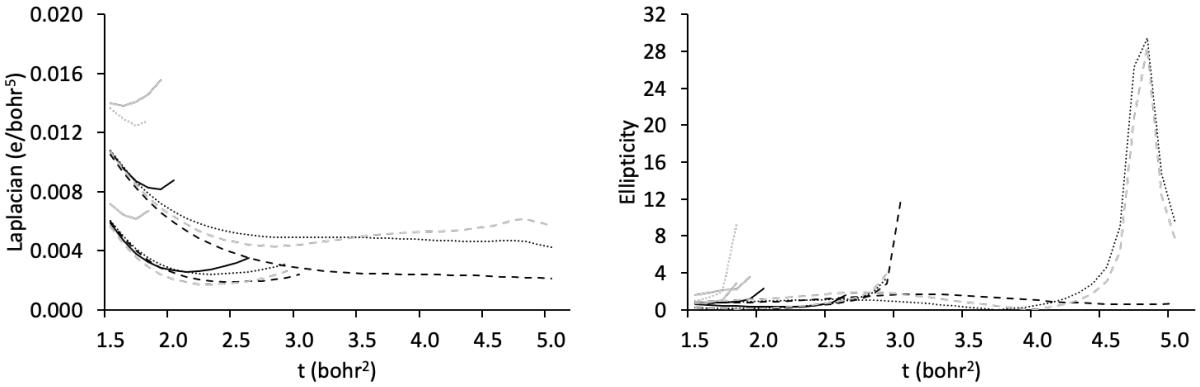

Figure SI9. Profiles of the Laplacian and the ellipticity as a function of *t* for the BCP trajectories involved in a $N_{cyano}\ldots C_{arom}$ interaction (CIGGII: plain black, CIGGEE_S: dashed black, CIGGEE: dotted black, CIGGII_Se: plain grey, CIGGOO: dotted grey, NOTECN: dashed grey).

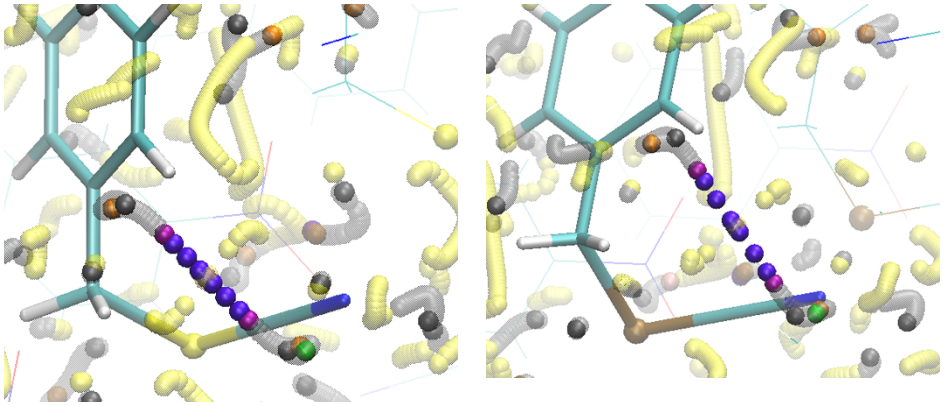

CIGGEE NOTECN

Figure SI10. BCPs depicting the conversion of the $N_{cyano}\ldots$arom to $N_{cyano}\ldots N_{cyano}$ interactions, BCP (pale yellow spheres) and RCP (pale grey spheres) trajectories. BCPs at t = 0.0, 1.5, 3.0, and 4.5 bohr² are shown in black, green, orange, and purple, respectively. The BCP position at t = 4.6 to 4.8 bohr² are displayed in dark blue.

Table SI1. BCPs involved in the various types of interactions involving aromatic (arom) and cyano groups. The corresponding atom…atom distance value is in parentheses (Å); $[t_i\text{-}t_f]\text{-}t_s$ is the trajectory length involving the BCP (bohr^2) followed by the t_s value (in italic) at which a RDG minimum is observed (bohr^2). Trajectories up to t = 5 bohr^2 are noted in bold.

	N_{cyano}…arom	N_{cyano}…CH_2	arom…arom	Other
S compounds				
CIGGII	[0.0-2.6] (3.39) [0.0-2.0]-*2.1* (3.43)	[0.0-1.7]-*1.8* (3.69)	/	/
CIGGEE_S	[0.0-3.0] (3.39) **[0.0-5.0] (3.55)**	[0.0-3.0]-*3.1* (4.75) [a]	[0.0-1.9]-*2.0* (3.76)	/
Se compounds				
CIGGEE	**[0.0-5.0] (3.55)** [0.0-2.9]-*3.0* (3.39)	/	[0.0-1.7]-*1.8* (3.76)	O_{nitro}…O_{nitro} [0.0-1.6] (3.21) [a]
CIGGII_Se	[0.0-1.9]-*2.0* (3.70) [0.0-1.8]-*1.9* (3.39)	/	/	/
CIGGOO	[0.0-1.8]-*1.9* (3.59)	/	[0.0-3.7]-*3.8* (3.72) [0.0-2.8]-*2.9* (3.77) [0.0-2.7]-*2.8* (3.84)	
Te compound				
NOTECN	**[0.0-5.0] (3.55)** [0.0-2.9]-*3.0* (3.36)	/	[0.0-1.7]-*1.8* (3.81)	/

[a] immobile

In addition to the BCPs described in the main text of the paper, several other types of interactions are frequently observed, such as those involving N_{cyano} and an aromatic ring (Table SI1, Figure SI7). They are observed in all structures and t_f does not appear to strongly depend on the atomic number Z. Particularly, in the isomorphous structures CIGGEE and NOTECN, each BCP involved in a complete trajectory merge with its inverse image at t = 5 bohr^2. Each of the four trajectories (2 BCPs and their inverse) starts between a N_{cyano} and a C_{arom} atom and then moves to the central position between two N_{cyano} atoms separated by a distance of 5.04 and 5.02 Å, respectively (Figure SI8). Such central positions are, in the unsmoothed EDD, seen as RCPs. In both crystal structures, the central BCP is surrounded by two almost perpendicular RCP trajectories at a minimal distance of 0.5-0.6 Å.

Located away from the chalcogen atoms, the BCP trajectories often end with a RDG minimum (Table SI1). It is especially verified for the weak aromatic…aromatic BCPs which all terminate before $t = 5$ bohr^2. In CIGGOO, a significant number of C_{arom}…C_{arom} BCPs appear due to the absence of nitro groups, while the number of N_{cyano}…C_{arom} BCPs is halved with respect to the other four structures. Indeed, there is only one BCP trajectory left (as well as its image) starting from N_{cyano} of the central molecule for CIGGOO compared to the other structures. Both BCP trajectories of CIGGII_Se are shorter than in the original structure CIGGII. All structures but CIGGOO actually involve a N_{cyano}…C_{arom} distance of about 3.36 to 3.39 Å. However, as already discussed, CIGGOO is the only system that involves chalcogen…N_{cyano} BCPs.

There is a complete N_{cyano}…C_{arom} BCP trajectory only for the series CIGGEE and CIGGEE_S, and NOTECN (Table SI1, Figure SI9). All values of L are positive, at all t, showing a permanent depletion in the ED. Two L profiles show a slight shoulder between $t = 4.6$ and 4.8 bohr^2. They correspond to larger position changes of the BCPs when moving with t (Figure SI10); they are clearly detected through maxima in the ellipticity profiles (Figure SI9). As for the aromatic…aromatic BCPs, a BCP trajectory which ends at $t_f < 5$ bohr^2 often meets a RCP trajectory at that particular value of t_f and further generates a RDG minimum (Table SI1). The isomorphous arrangement of the series CIGGEE_S, CIGGEE, and NOTECN, favors the presence of a complete N_{cyano}…aromatic BCP trajectory (Table SI1).